β-Barrel Mobility Underlies Closure
of the Voltage-Dependent Anion Channel

Ulrich Zachariae,[1,3,7] Robert Schneider,[2,4,7] Rodolfo Briones,[1] Zrinka Gattin,[2] Jean-Philippe Demers,[2] Karin Giller,[2] Elke Maier,[5] Markus Zweckstetter,[2] Christian Griesinger,[2] Stefan Becker,[2] Roland Benz,[5,6] Bert L. de Groot,[1,*] and Adam Lange[2,*]

[1]Computational Biomolecular Dynamics Group
[2]Department of NMR-based Structural Biology
Max Planck Institute for Biophysical Chemistry, Am Fassberg 11, 37077 Göttingen, Germany
[3]SUPA, School of Physics and Astronomy, The University of Edinburgh, King's Buildings, Edinburgh EH9 3JZ, UK
[4]Protein Dynamics and Flexibility by NMR, Institut de Biologie Structurale, 41 rue Jules Horowitz, 38027 Grenoble, France
[5]Rudolf Virchow Center, DFG Research Center for Experimental Biomedicine, University of Würzburg, Versbacher Str. 9, 97078 Würzburg, Germany
[6]School of Engineering and Science, Jacobs University Bremen, Campusring 1, 28759 Bremen, Germany
[7]These authors contributed equally to this work
*Correspondence: bgroot@gwdg.de (B.L.d.G.), adla@nmr.mpibpc.mpg.de (A.L.)
http://dx.doi.org/10.1016/j.str.2012.06.015

SUMMARY

The voltage-dependent anion channel (VDAC) is the major protein in the outer mitochondrial membrane, where it mediates transport of ATP and ADP. Changes in its permeability, induced by voltage or apoptosis-related proteins, have been implicated in apoptotic pathways. The three-dimensional structure of VDAC has recently been determined as a 19-stranded β-barrel with an in-lying N-terminal helix. However, its gating mechanism is still unclear. Using solid-state NMR spectroscopy, molecular dynamics simulations, and electrophysiology, we show that deletion of the rigid N-terminal helix sharply increases overall motion in VDAC's β-barrel, resulting in elliptic, semicollapsed barrel shapes. These states quantitatively reproduce conductance and selectivity of the closed VDAC conformation. Mutation of the N-terminal helix leads to a phenotype intermediate to the open and closed states. These data suggest that the N-terminal helix controls entry into elliptic β-barrel states which underlie VDAC closure. Our results also indicate that β-barrel channels are intrinsically flexible.

INTRODUCTION

The voltage-dependent anion channel (VDAC) is the most abundant protein in the outer mitochondrial membrane of eukaryotes, where it mediates permeation of ATP, ADP, and other essential metabolites (Benz, 1994; Colombini, 2004). It is also considered to be a key player in the mitochondrial pathway of apoptosis (Shoshan-Barmatz et al., 2008, 2010). In the presence of transmembrane voltages higher than about 30 mV, independent of their polarity, VDAC exhibits a complex gating process to one or more subconductance ("closed") states that are impermeable

to ATP and exhibit altered ion selectivity (Benz, 1994; Colombini, 1989, 2004). After three decades of experimental study, recent work on crystallized and detergent-solubilized protein has revealed the three-dimensional structure of the VDAC1 isoform to be a 19-stranded β-barrel with a partly helical N-terminal region situated within the aqueous pore (Bayrhuber et al., 2008; Hiller et al., 2008, 2010; Ujwal et al., 2008). So far, however, the nature of VDAC's gating process has remained elusive from both experimental and computational studies (Bayrhuber et al., 2008; Choudhary et al., 2010; Hiller et al., 2008, 2010; Lee et al., 2011; Rui et al., 2011; Ujwal et al., 2008). The N terminus of VDAC has been shown to be crucial for channel gating (Song et al., 1998; Thomas et al., 1993) as well as for interaction with apoptosis-related proteins (Abu-Hamad et al., 2009; Shoshan-Barmatz et al., 2008). However, several studies have indicated that conformational rearrangements within the β-barrel may be involved in gating as well (Mannella, 1997; Peng et al., 1992; Zimmerberg and Parsegian, 1986). In particular, it was found that gating is strongly influenced by osmotic pressure applied on the bilayer. From this finding, a substantial internal volume change during gating was inferred, pointing to a large reconfiguration of channel geometry (Zimmerberg and Parsegian, 1986). Gating is regulated by small molecules as well as apoptotic and antiapoptotic proteins (Benz, 1994; Colombini, 1989, 2004; Shoshan-Barmatz et al., 2008, 2010). A molecular understanding of the gating process is thus not only of mechanistic interest but also holds promise for further elucidation of the role of VDAC in mitochondrial apoptosis.

We have recently demonstrated that the N terminus assumes a well-defined conformation and plays a stabilizing role for VDAC1 (Schneider et al., 2010a). β strands in contact with the N terminus are less dynamic than others (Villinger et al., 2010), and removal of the N terminus affects the conformation of the β-barrel (Schneider et al., 2010a). On the other hand, VDAC1's β-barrel frame can exhibit extensive breathing motions (Villinger et al., 2010). Mutations of a glutamate residue (Glu73) whose side chain points toward the lipid bilayer affect both the dynamic behavior of the β-barrel and the gating properties of the channel (Villinger et al., 2010; Zaid et al., 2005). Consequently, local
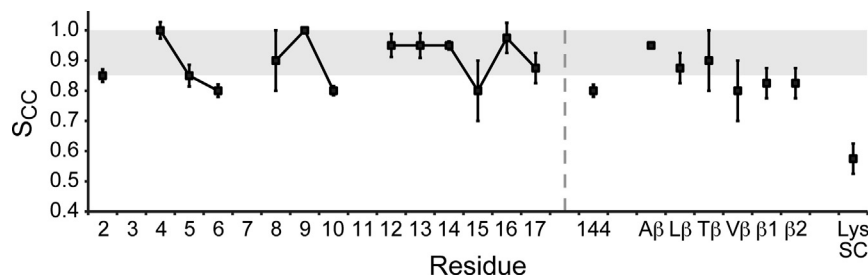
Figure 1. S_{CC} Order Parameters Measured on hVDAC1 in Lipid Bilayers

All values refer to Cα-Cβ correlations except "Lys SC," which corresponds to lysine Cδ-Cε side-chain correlations as a reference for mobile moieties. For comparison of mobility in the N terminus and in the β-barrel, overall Cα-Cβ order parameters of alanine, leucine, threonine, and valine residues in β strand conformation (whose resonances overlap) are also shown (labels "Aβ," "Lβ," "Tβ," "Vβ"), as well as average Cα-Cβ order parameters for other β strand residue types whose resonances overlap in two broad spectral regions (Cα shifts around 55 ppm, Cβ shifts around 35 ppm; labels "β1," "β2"). Error bars are based on Monte Carlo simulations, where estimates of the experimental error were obtained from spectral noise (see Supplemental Experimental Procedures).The order parameter range from 0.85 to 1 is indicated by a gray-shaded bar. A vertical dashed line separates S_{CC} values of N-terminal residues (left) from values of residues in other parts of the molecule. See also Table S1 and Figures S4 and S5.

mobility and stability within VDAC1 can be expected to play an important role for channel gating.

As the membrane environment is generally found to be important for the structure and function of membrane proteins, studies that explicitly take the lipid membrane into account are essential (Ader et al., 2008; Hunte and Richers, 2008; Nietlispach and Gautier, 2011; Phillips et al., 2009). We have therefore investigated the dynamics of VDAC1 and its role in gating in lipid bilayers, using a combination of solid-state NMR spectroscopy, electrophysiology, and molecular dynamics (MD) simulations. We quantify molecular mobility in bilayer-embedded VDAC1 and examine the effect of removal of the N terminus on the conformation of the β-barrel. Furthermore, we demonstrate the importance of specific contacts between the β-barrel and the N-terminal helix for the overall stabilizing role of the latter. We show that only a large-scale conformational transition of the barrel scaffold itself can explain the large drop in conductance upon closure and the concomitant change in ion selectivity. Changes in conductance and selectivity observed in simulations of VDAC1 at different degrees of closure are in quantitative agreement with experimental data. The combination of experimental and simulation results hence allows us to suggest both a mechanism of VDAC closure and a molecular model for the closed states of VDAC. This mechanism provides a simple explanation for the observed dependence of gating on membrane pressure. Our results challenge the common belief that β-barrel channels are generally characterized by high structural rigidity.

RESULTS

The N Terminus Does Not Exhibit Large Dynamics on the Sub-ms Timescale

Data reported in Schneider et al., 2010a indicated that the N terminus of human VDAC1 (hVDAC1) does not exhibit large-scale mobility. To investigate this finding quantitatively, we measured (^{13}C,^{13}C) dipolar order parameters (S_{CC}) for residues in the N terminus as well as in other parts of the molecule using double-quantum (2Q) solid-state NMR spectroscopy as introduced in Schneider et al., 2010b. This technique is sensitive to dynamics on the picosecond (ps) to millisecond (ms) timescale. Because of the considerable size of hVDAC1 and the large number of residues in β sheet conformation, spectral overlap precludes identification of residue-specific order parameters

for a large part of the molecule. To estimate overall mobility in the β-barrel, we also analyzed overlapping signals of residues in β strand secondary structure and determined average order parameters for these.

Results displayed in Figure 1 and Table S1 (available online) show that backbone S_{CC} order parameters in the N terminus are in the same range as, or higher than, average values found for residues in the β-barrel. Most measured values in the N terminus range between 0.85 and 1, on the rigid end of the dynamics scale. Lower S_{CC} values are found in residues Thr6, Leu10 in the helix kink, and Arg15. Thus, local mobility is present in the hVDAC1 N terminus. However, our data show that, globally, the N terminus is certainly not more dynamic than the β-barrel on a sub-ms timescale. Peak broadening or doubling, which would indicate dynamics on slower timescales, is not observed, further confirming the well-defined structure of the hVDAC1 N terminus (Schneider et al., 2010a; Villinger et al., 2010). However, it may be possible that other highly dynamic conformations not accessible to solid-state NMR experiments exist in equilibrium.

Additionally, on a timescale of about 300 ns, the dynamics of mouse VDAC1 (mVDAC1, see also Supplemental Experimental Procedures) were studied in MD simulations. mVDAC1, which differs from hVDAC1 in four amino acid residues, was chosen for MD simulations because of the availability of a high-resolution crystal structure (Ujwal et al., 2008). Figure 2A shows the backbone root-mean-square fluctuations (rmsf) of wild-type (WT-) mVDAC1 (black curve). Rmsf minima correspond to the centers of β strands 1–19. These define a baseline of maximal structural rigidity (cyan line in Figure 2A), which is slightly raised across β1–β6 and in β19. The N-terminal helix (red-shaded area) exhibits a low fluctuation level, comparable to the central residues of the β strands. The rmsf of short interstrand loops and some strand termini exceeds that of the body of the N-terminal helix by a factor of 2 to 3 (color-coded in Figure 2B). The MD results therefore show that the N-terminal helix is relatively rigid under equilibrium conditions on a timescale of up to hundreds of nanoseconds, in agreement with the NMR data.

Removal of the N Terminus Induces Structural Instability

Recombinant WT-hVDAC1 exhibits a major open-state conductance of about 4 nS (Figure S1) and a voltage-dependence of membrane current typical for VDAC channels (Benz, 1994; Colombini, 1989, 2004). Deletion of most or all of the 20 N-terminal
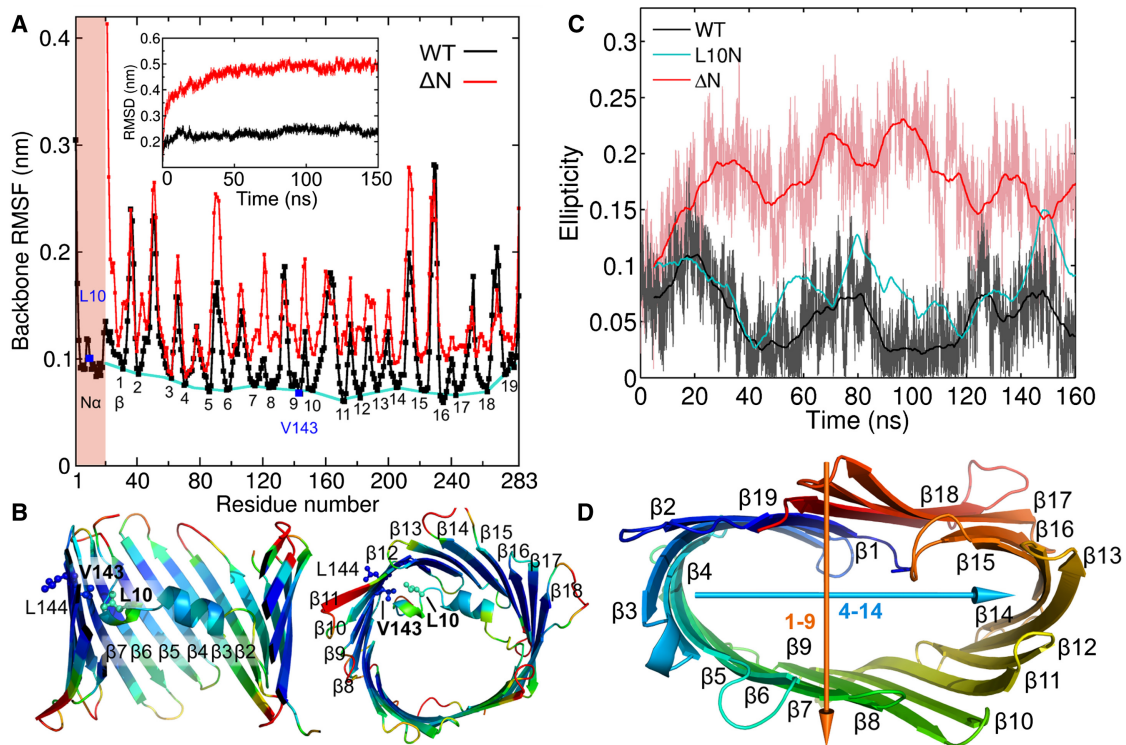
Figure 2. Flexibility and Conformational Changes of the mVDAC1 β-Barrel

(A) Rmsf distribution in WT- (black) and Δ(1–20)-mVDAC1 (red). (Cyan) Baseline of minimal rmsf across the barrel. (Inset) Rmsd of WT- (black) and Δ(1–20)-mVDAC1 (red) with respect to the initial structure under a membrane surface tension of −45 mN/m.

(B) Rmsf of mVDAC1 in MD simulations, color-coded on the structure from blue (low) to red (high). Parts of strands 9–18 are cut away for clarity (left).

(C) Ellipticity of WT- (black), L10N- (cyan), and Δ(1–20)-mVDAC1 (red) without additional membrane pressure.

(D) Partial collapse of the Δ(1–20)-mVDAC1 barrel under low uniaxial membrane stress (∼−10 mN/m) occurs preferentially along an axis approximately running through β strands 1–9 rather than in the perpendicular direction. β strands 1 to 19 are color-coded from blue to red. See also Figure S4.

residues in *Neurospora crassa* VDAC (ncVDAC) has been shown to lead to noisier recordings in electrophysiology, affect or abolish voltage gating, and reduce channel conductance (Popp et al., 1996; Runke et al., 2006). This also applies to hVDAC1 (De Pinto et al., 2008; Schneider et al., 2010a). Lipid bilayer measurements on an hVDAC1 N-terminal truncation variant (Δ(1–20)-hVDAC1) show noisy traces with no apparent voltage gating and a distribution of current steps with a broad maximum between G = 0.5 nS and G = 2.5 nS (Figure S1). In solid-state NMR experiments on hVDAC1 in lipid bilayers, N-terminal truncation leads to disappearance of resonance signals from β strand 9, which forms a hydrophobic contact with Leu10 in the N-terminal helix (Figure S2) (Schneider et al., 2010a).

The findings of increased channel noise and disappearing resonance signals point to increased dynamics and reduced structural stability in N-terminally truncated hVDAC1. To test this hypothesis, we performed equilibrium MD simulations of Δ(1–20)-mVDAC1 in a dimyristoyl phosphatidylcholine (DMPC) lipid bilayer and compared its behavior to the wild-type. As Figure 2A shows, the overall fluctuation level is substantially raised in the deletion mutant (red curve). In particular, the difference in the rmsf baseline between β strands 5–19 is remarkable, as it demonstrates that a major portion of the wild-type β-barrel had

been stabilized by the presence of the N-terminal helix. Elliptic fits of the β-barrel scaffold demonstrate an increased tendency of Δ(1–20)-mVDAC1 to adopt a more elliptic geometry than the wild-type (Figure 2C). The global breathing motion of the barrel (Villinger et al., 2010) is evident from fluctuations of the average ellipticity occurring on a timescale of 30–50 ns, both in Δ(1–20)- and WT-mVDAC1.

It has been demonstrated that tension of biological membranes can modulate the shape and function of membrane proteins (Perozo et al., 2002; Schmidt and MacKinnon, 2008). We therefore investigated the behavior of Δ(1–20)- and WT-mVDAC1 under low to medium membrane surface tension in MD simulations. A substantial difference between Δ(1–20)- and WT-mVDAC1 was observed. Figure 2A (inset) displays the development of the root-mean-square deviation (rmsd) from the initial structure at a membrane surface tension of −45 mN/m, applied isotropically in the x-y plane. These data show that Δ(1–20)-mVDAC1 is perturbed by membrane tension more strongly than the wild-type. Structural analysis revealed that this deviation results from a global transition of the β-barrel of the deletion mutant into a smaller, more elliptic shape (Figure 2D). In WT-mVDAC1, this transition is largely inhibited by the N-terminal helix. Interestingly, in cases of uniaxial shear stress applied on the membrane, the transition is direction-dependent. The

β-barrel of Δ(1–20)-mVDAC1 is more susceptible to deformation along an axis passing through β strands 1 and 9 than in the perpendicular direction connecting β strands 4 and 14 (Figure 2D). Substantial deformation along the former axis can already be induced by relatively small values of surface tension on the order of −10 mN/m. This magnitude of surface tension is in the range biologically relevant for, for example, mechanosensitive channels (Martinac et al., 1987; Sukharev, 2002) and close to values observed in thermal membrane undulations of planar lipid bilayers (Hirn et al., 1999). The wild-type N-terminal helix, running alongside of β strands 10–17, is thus located at a position where it maximally stabilizes the barrel structure. Nevertheless, the wild-type barrel is also prone to deformation, despite the stabilizing effect of the N-terminal helix. Here, elliptic states can be obtained by applying a slightly larger surface tension of about −15 mN. The ellipticity of the Δ(1–20)-mVDAC1 β-barrel observed in low-stress simulations converges to a value of about 0.5, which we will call a *semicollapsed* state in the following. Note that this state corresponds to a broad ensemble of structures.

Electrophysiology Calculations

We hypothesized that the elliptic deformation of the β-barrel seen in our simulations could provide an explanation for the changes in electrophysiology parameters observed experimentally in the N-terminal deletion mutant. MD simulations have been successfully used to characterize ion flux in bacterial porins (Pongprayoon et al., 2009; Tieleman and Berendsen, 1998). Using our newly developed computational electrophysiology scheme (Kutzner et al., 2011), we atomistically simulated ion flux through WT- and Δ(1–20)-mVDAC1 under transmembrane potential gradients close to experimental values (Figure 3A, inset). From the individual fluxes of anions and cations, selectivity and conductance values of VDAC1 were calculated.

In our simulations, WT-mVDAC1 displayed a conductance of G = 4.2 ± 0.2 nS (SEM) in 1M KCl, in close agreement with the experimental value for WT-hVDAC1 (about 4 nS, see Figures 3A and S1; Abu-Hamad et al., 2009; Benz, 1994; Runke et al., 2006). The ion selectivity for WT-mVDAC1 was calculated by statistical averaging over the ratio of permeating anions (p_-) and cations (p_+) in 20 ns windows taken from the trajectories, yielding p_-/p_+ = 1.7 ± 0.4 (SEM) (Figure 3B), also in good agreement with experiment (p_-/p_+ = 2.2). Removal of the N-terminal helix, in the absence of further structural changes, results in a larger pore; accordingly, a raised conductance of 6.7 ± 0.3 nS (SEM) was observed for Δ(1–20)-mVDAC1 at a similar p_-/p_+ ratio of 1.6 ± 0.4 (SEM). We then examined conductance levels of the partially collapsed, elliptic states of Δ(1–20)- and WT-mVDAC1 formed under low to medium membrane tension.

Figure 3A shows the conductance of Δ(1–20)-mVDAC1 relative to the ellipticity of the β-barrel. Near ellipticity values of 0.4–0.5, a sharp transition is observed that reduces the conductance to 1.5–2 nS (Figure 3A). Similar results were obtained for the elliptic, semicollapsed states of WT-mVDAC1 with the N terminus present within the barrel (Figure 3A). Conductance values calculated for molecules with ellipticities between 0.3 and 0.4 were in the range of values found experimentally for the closed state of VDAC. The fact that a drop in conductance is only seen upon such large deformations of the barrel suggests
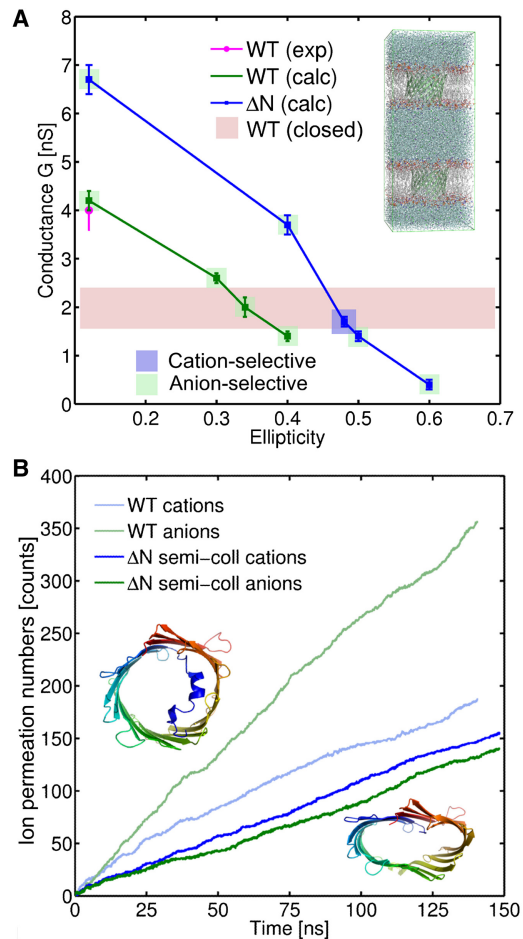
Figure 3. Ion Flux and Conductance through WT and Δ(1–20)-mVDAC1

(A) Conductance of WT- (green) and Δ(1–20)-mVDAC1 (blue) in relation to elliptic distortion of the beta barrel scaffold, calculated from computational electrophysiology simulations. Background shading of the data points indicates the ion selectivity of the corresponding mVDAC1 states (light green, anion-selective; light blue, cation-selective). The magenta data point corresponds to the experimental conductance of open WT-hVDAC1, whereas the experimentally determined average conductance of the closed state of WT-hVDAC1 is indicated by a red-shaded bar. Error bars reflect standard error of the mean (SEM).
(B) Representative ion flux and selectivity for cations and anions of open WT- (light colors) and semicollapsed Δ(1–20)-mVDAC1 (solid colors) at a transmembrane potential elicited by a charge imbalance of 2 e⁻ across the membrane. The ellipticity of semicollapsed Δ(1–20)-mVDAC1 was 0.47. See also Figure S3.

that a significant structural change is required to elicit the magnitude of channel conductance decrease detected experimentally. In terms of conductance, semicollapsed states may thus explain voltage-induced entry into subconductance states of VDAC1. Importantly, these states can also explain the magnitude of volume loss upon closure, which has been measured to be in the order of 10^4 $Å^3$ (Zimmerberg and Parsegian, 1986). In our simulations, semicollapsed states of Δ(1–20)-mVDAC1 exhibit a volume reduction of about 1 × 10^4 $Å^3$ compared to the open state of WT-mVDAC1.

As mentioned above, the average conductance measured experimentally for Δ(1–20)-hVDAC1 closely resembles that reported for the closed state of VDAC1 variants (Benz, 1994; Colombini, 1989, 2004). However, Δ(1–20)-hVDAC1 exhibits slightly increased anion selectivity in lipid bilayer experiments (p_-/p_+ about 2.6 in Δ(1–20)-hVDAC1 versus 2.2 in WT-hVDAC1), whereas the closed state of VDAC1 is typically reported to be cation-selective (Benz, 1994; Choudhary et al., 2010; Colombini, 2004). Notably, this trend is similar to the one observed in the N-terminal deletion mutant Δ(3-20) of ncVDAC (p_-/p_+ of about 2 versus 1.3 for WT-ncVDAC; Popp et al., 1996; Runke et al., 2006). Consequently, we investigated whether the selectivities of the semicollapsed conformations of Δ(1–20)- and WT-mVDAC1 in our simulations could explain those experimental observations. We found that the calculated ionic selectivities of the elliptic states are crucially dependent on the precise geometry of the pore. The charge state of the N-terminal residue of Δ(1–20)-mVDAC1 (Gly21), which protrudes into the channel at the center of the pore, plays a minor, additional role. Importantly, Met1 in the wild-type is situated distant from the pore center, such that WT-hVDAC1 does not have a charge at this position.

Most of the elliptic states display clear anion selectivity, with selectivity values around $p_-/p_+ = 1.5$. However, the ionic selectivity of Δ(1–20)-mVDAC1 switches to nonselective or slightly cation selective states near a conductance of about 1.7 nS. In particular, semicollapsed forms with an ellipticity near 0.47 exhibit a conductance of 1.7 ± 0.1 nS (SEM), and these states are found to be cation-selective with $p_-/p_+ = 0.7$ when the N-terminal Gly21 residue is uncharged, as it would be in the full-length protein (Figure 3B). This ellipticity is close to the convergence value of the deletion mutant under low membrane stress.

Notably, no switch in ion selectivity was observed for semicollapsed states of WT-mVDAC1. In the full-length protein, these states are actually rather characterized by increased anion selectivity. This finding suggests that the presence of the N-terminal helix within the barrel, with its excess of positive charge, prevents the switch from anion to cation selectivity observed experimentally during VDAC gating. This hypothesis is corroborated by an analysis of the potential of mean force (PMF) for cations and anions traversing the VDAC pore (Figure S3). The major barrier for cation translocation in the wild-type originates from the presence of the N-terminal helix about 6 Å from the center of mass of the channel. In the PMF for Δ(1–20)-mVDAC1 in the semicollapsed state, this barrier is obviously absent, and only a slight preference for anions is expected to remain. However, the permeability difference between cations and anions leads to cation selectivity at certain ellipticities. Taken together, semicollapsed states with no N terminus inside can thus account for the selectivity of both the N-terminal deletion mutant and the closed state of the full-length protein, depending on pore geometry and charge.

The L10N Mutant Displays Intermediate Behavior between WT and Δ(1–20)-hVDAC1
Our data so far have shown that the N terminus plays a stabilizing role for the entire VDAC1 β-barrel and that the conformation of the barrel is closely related to its conductance and selectivity. In previous studies, the N terminus of human and mouse

VDAC1 was found to be attached to the barrel wall via a network of hydrogen bonds as well as a hydrophobic contact between Leu10 in the N terminus and a hydrophobic patch involving residues Val143 and Leu150 in β strands 9 and 10 (Hiller et al., 2008; Schneider et al., 2010a; Ujwal et al., 2008). This hydrophobic interaction appears to be largely conserved across species, as indicated by a recent sequence alignment study (Young et al., 2007). To investigate experimentally the relative importance of these interactions and the effect of mutations destabilizing N-terminal attachment to the barrel, we expressed a mutant hVDAC1 variant with Leu10 exchanged for asparagine. We thus used a conservative mutation that selectively disrupts the hydrophobic contact. In solid-state NMR spectra of L10N-hVDAC1, the pattern of resonances, including those from the N terminus, is very well preserved, indicating correct folding of the mutant protein (Figure S2). However, striking differences in intensity are visible in signals from the N terminus (Figure 4A) as well as from β strand 9 (Figure 4B). A systematic analysis of signal intensities and linewidths shows that signals from the N terminus and β strand 9 are selectively and significantly attenuated (Figures 4C and S4), suggesting increased dynamics in these residues. Signal linewidths, on the other hand, increase slightly but in a similar manner for the N terminus and other regions (Figure 4D). These data confirm the crucial role of the hydrophobic contact between Leu10 and the region around Val143 for attachment of the N terminus to the β-barrel wall and point to an elevated level of structural or dynamical disorder specifically in N terminus and β strand 9 of L10N-hVDAC1.

Next, we analyzed the electrophysiological characteristics of L10N-hVDAC1 in bilayer measurements. Figure 4E shows that the mutant forms stable, voltage-gated pores. Importantly, however, already at a transmembrane voltage of 10 mV, where WT-hVDAC1 is predominantly open with a major conductance of about 4 nS (Figure S1), L10N-hVDAC1 exhibits a dominant conductance of 2 nS (Figures 4E and 4F), a value resembling the closed state of WT-hVDAC1 and the observable conductance state of the N-terminal deletion mutant Δ(1–20)-hVDAC1. Also, L10N-hVDAC1 shows a voltage-dependence of conductance which is intermediate to WT- and Δ(1–20)-hVDAC1 (Figure 5). These observations are in line with the hypothesis that disruption of the hydrophobic contact Leu10-Val143 facilitates dynamical and/or conformational changes that allow entry of hVDAC1 into a closed state. However, note that, similar to Δ(1–20)-hVDAC1, L10N-hVDAC1 exhibits increased selectivity for anions over cations (p_-/p_+ about 3.2 in L10N-hVDAC1 versus 2.2 in WT-hVDAC1).

In MD simulations of L10N-mVDAC1, no significant deviations from the behavior of WT-mVDAC1 were observed under equilibrium conditions (see, e.g., Figure 2C, cyan curve). To reproduce the effect of a transmembrane voltage on the N terminus, we used force-probe MD simulations to investigate its behavior under mechanical forces corresponding to those exerted on charged residues by a transmembrane electric field. The N-terminal helix has a surplus of two positive charges, rendering its position sensitive to an electric field. To make the effects of applied forces accessible within the timescale of our MD simulations, we used forces corresponding to electric fields raised by one to two orders of magnitude over physiological values. In multiple 150 ns simulations in which a transmembrane voltage
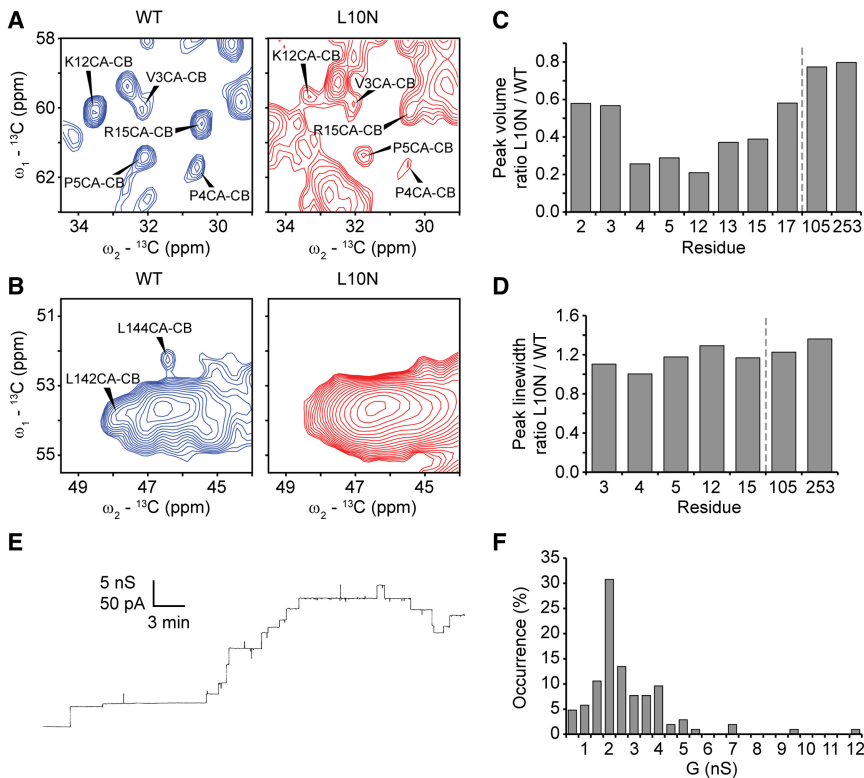
Figure 4. Solid-State NMR and Electrophysiological Data from L10N-hVDAC1

(A and B) Comparison of cross-peak intensities in WT- and L10N-hVDAC1. Shown are regions of (^{13}C,^{13}C) PDSD correlation spectra (15 ms mixing time) displaying resonances from N terminus (A) and β strand 9 (B). See also Figure S2. Blue, WT; red, L10N-hVDAC1.

(C) Ratios of normalized Cα-Cβ cross-peak volumes between (^{13}C,^{13}C) PDSD spectra (15 ms mixing time) recorded on L10N- and WT-hVDAC1. In L10N-hVDAC1, normalized cross-peak volumes are significantly more attenuated in the N terminus than in control residues 105 and 253 (p = 0.0002, two-sided t test, unequal variances assumed). See also Figure S4.

(D) Ratios of average Cα-Cβ cross-peak linewidths between 15 ms (^{13}C,^{13}C) PDSD spectra of L10N and WT hVDAC1. Average peak linewidths increase slightly in L10N hVDAC1 spectra but not differentially for residues in the N terminus and control residues (p = 0.22, two-sided t test, unequal variances assumed).

(E) Single-channel recordings of L10N-hVDAC1 inserted into lipid bilayers. Applied voltage was 10 mV.

(F) Histogram of conductance values (G) observed on L10N-hVDAC1 in lipid bilayers at a transmembrane voltage of 10 mV. See also Figure S1.

of about 2 V was modeled, the L10N-mutated helix detached from the mVDAC1 β-barrel with an average time constant of 66 ± 40 ns (SEM). In contrast, no extraction of the N-terminal helix from the β-barrel scaffold was seen in WT-mVDAC1 at forces corresponding to this voltage. The wild-type helix could also be detached on a timescale of a few hundreds of nanoseconds, but higher forces corresponding to transmembrane voltages above 3 V were necessary. Thus, in experiment as well as simulation, the hydrophobic interaction between Leu10 and the hydrophobic patch around Val143 appears to be key to stabilizing the position of the wild-type N-terminal helix within the β-barrel, whereas the L10N mutant enters into a collapsed state more easily.

DISCUSSION

One of the longest-standing questions related to the β-barrel channel VDAC is the nature of its gating process which can be induced by transmembrane voltages above ±30 mV and by apoptotic and antiapoptotic proteins (Benz, 1994; Colombini, 1989, 2004; Shoshan-Barmatz et al., 2008, 2010). In the present study, we aimed for mechanistic insight into the gating process, based on the atomic structure of VDAC.

In the first X-ray crystallographic study of a porin, it was noted that β-barrel channels should be deformable because of their hull-like architecture (Cowan et al., 1992). However, trimeric bacterial porins have a substantial hydrophobic core at their trimer interfaces, which explains their stability against denaturation and proteolysis (Cowan et al., 1992). The notion that β-barrel membrane proteins have a particularly high level of

rigidity has thus entrenched over time, although it essentially stems from the stability of trimeric bacterial porins toward unfolding (Haltia and Freire, 1995; Wimley, 2003). Most trimeric porins show voltage-dependent gating in planar bilayer experiments at markedly raised transmembrane potentials (about ±100mV; Dargent et al., 1986; Lakey and Pattus, 1989; Schindler and Rosenbusch, 1981). In contrast to bacterial porins (Cowan et al., 1992; Zachariae et al., 2006), however, VDAC does not display a clearly localized area of intimate trimer contact (Bayrhuber et al., 2008; Ujwal et al., 2008). It was hypothesized earlier that this could enhance the dynamics of the entire barrel, which may in turn play a role in the propensity of VDAC to undergo gating (Mannella, 1997).

In this study, we first quantified and confirmed the overall rigid nature of the hVDAC1 N terminus by measuring S_{CC} order parameters of the backbone. Using MD simulations, we then developed a molecular description of the effects of N-terminal truncation on the VDAC1 β-barrel. In electrophysiology, deletion of the N-terminal helix is found to increase channel noise, reduce conductance, and, most importantly, abolish voltage gating, whereas in solid-state NMR spectra, the deletion leads to loss of resonance signals also from residues within the barrel. Our results suggest that removal of the N-terminal helix results in a highly dynamic mutant VDAC1 channel which exhibits an increased propensity to enter semicollapsed, elliptic states with conductance levels similar to those found in the closed state of the wild-type channel. Such semicollapsed barrel states are also accessible in the presence of the N-terminal helix albeit with reduced propensity. These findings demonstrate not only the importance of the N-terminal helix in voltage gating but
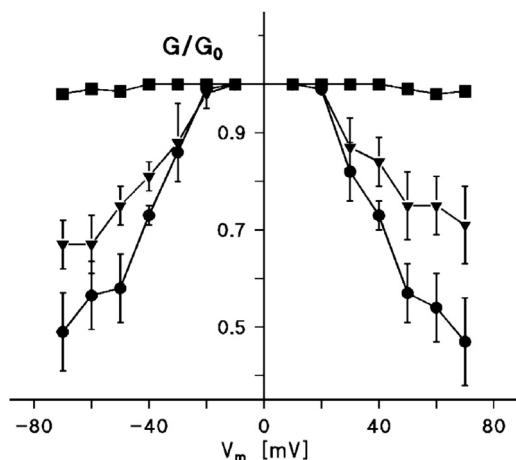
Figure 5. Lipid Bilayer Conductance Values of the Different hVDAC1 Variants Investigated

Shown are ratios of the conductance G at a given membrane potential (V_m) divided by the conductance G_0 at 10 mV as a function of the membrane potential V_m. Circles, WT-hVDAC1; triangles, L10N-hVDAC1; squares, Δ(1–20)-hVDAC1. The membrane potential always refers to the cis-side of the membrane. Means ± SD of three membranes are shown for each hVDAC1 variant. See also Figure S1.

also for stabilizing the open state of the pore by virtue of its rigidity. In addition, we found that this stabilizing effect hinges upon a major attachment point of the helix to the barrel wall at the hydrophobic Leu10-Val143 contact. Weakening of this contact in L10N-hVDAC1 leads to a phenotype characterized by a reduction of the gating voltage at which the channel enters predominantly into a closed state with a conductance of about 2 nS (Figures 4E, 4F, and 5).

Our observations suggest a scenario in which an ensemble of semicollapsed, elliptic geometries of the VDAC1 β-barrel underlie the subconductance states observed experimentally under elevated transmembrane voltages. Our finding that large deformations of the VDAC1 β-barrel are required to account for the reduction in conductance observed experimentally is in excellent agreement with the observation of a volume reduction in the order of 10^4 Å^3 during closure (Zimmerberg and Parsegian, 1986). Such a volume change would be inconsistent with a more local conformational change. Similarly, a recent VDAC1 study using continuum electrostatics calculations demonstrated that movement of the N terminus alone, even if leading completely out of the β-barrel, is unlikely to account for VDAC1 gating (Choudhary et al., 2010). According to our data, such a movement of the N terminus should also lead to destabilization of the barrel. Gating models involving only a movement of the N terminus, without a concomitant effect on the barrel, thus appear unlikely. Conversely, our data are well in line with the observation of extensive dynamics and a pronounced breathing motion in the hVDAC1 β-barrel by both solution-state NMR and MD simulations (Villinger et al., 2010). A gating mechanism by semicollapse of the pore is also consistent with the observed dependence of gating on osmotic pressure (Zimmerberg and Parsegian, 1986) and on the presence of nonlamellar lipids, which increase lateral pressure, in the surrounding membrane (Rostovtseva et al.,

2006). Thus, a coherent mechanism underlying VDAC gating emerges that explains a wide range of experimental data.

Our simulations show that semicollapsed barrel states can also account for the switch in ion selectivity observed upon gating, depending on pore geometry and charge. In our simulations of Δ(1–20)-mVDAC1, anion selectivity is preserved in most of the subconductance states, in agreement with experimental data. Δ(1–20)-mVDAC1 then switches to cation selectivity at barrel ellipticity values of about 0.47, where the barrel exhibits a conductance of about 2 nS, similar to the closed state of WT-hVDAC1. Cation selectivity is not observed, however, in semicollapsed states of WT-hVDAC1 which retain the N-terminal helix within the barrel, because of the presence of an excess of positively charged residues in the N terminus.

Hence, our data are consistent with a voltage-dependent motion of the N-terminal helix, partially or fully detaching it from the β-barrel, as a possible mechanism to control entry of VDAC1 into the closed state (Figure 6). More specifically, the attenuation of signals from the N terminus in solid-state NMR spectra of the L10N-hVDAC1 mutant may be due to increased overall motion in this region or, alternatively, exchange between two states, namely, the relatively rigid wild-type conformation and a more mobile or disordered N terminus which is not visible in the solid-state NMR spectra. Notably, such a mobile population may well also be present in wild-type VDAC1 albeit to a smaller extent. The absence of chemical shift changes or linewidth increases in N-terminal resonances of L10N-hVDAC1 indicates that such exchange between different states of the N terminus would have to be slow relative to the NMR chemical shift timescale (milliseconds), in agreement with electrophysiology data for the timescale of VDAC gating (Colombini, 1989). In our simulations, a force corresponding to a transmembrane voltage about two orders of magnitude higher than values used experimentally is sufficient to remove the N terminus of hVDAC1 from the pore on a nanosecond timescale. Our results thus suggest that displacement of the charged N-terminal helix of hVDAC1 by transmembrane voltages in the range of tens of millivolts is possible on the timescale of gating. Previous accessibility studies have also indicated that it is in principle possible for the helix to leave the barrel (De Pinto et al., 1991; Guo et al., 1995). In such a state, the N terminus may become disordered or bind to the lipid membrane, as indicated by earlier reports (De Pinto et al., 2007; Mannella, 1998).

It is important to note, however, that our data do not imply that removal of the helix from the barrel is required for VDAC gating. As our simulations of full-length VDAC1 show, partial collapse and the associated reduction in conductance can also be achieved by conformational changes within the barrel alone while the N terminus remains inside. These results are in full agreement with a recent study showing that attachment of the mVDAC1 N terminus to the barrel wall via disulfide linkage does not prevent voltage gating, suggesting a gating mechanism via partial barrel collapse (Teijido et al., 2012). Similarly, another study found that antibodies directed against the N terminus have no influence on gating properties of hVDAC1, also pointing to conformational changes within the barrel as primary gating mechanism (Benz et al., 1992). It is noteworthy that, in the work of Teijido et al. (2012), residue Leu10, which we have identified as an important anchor of the N terminus to a hydrophobic
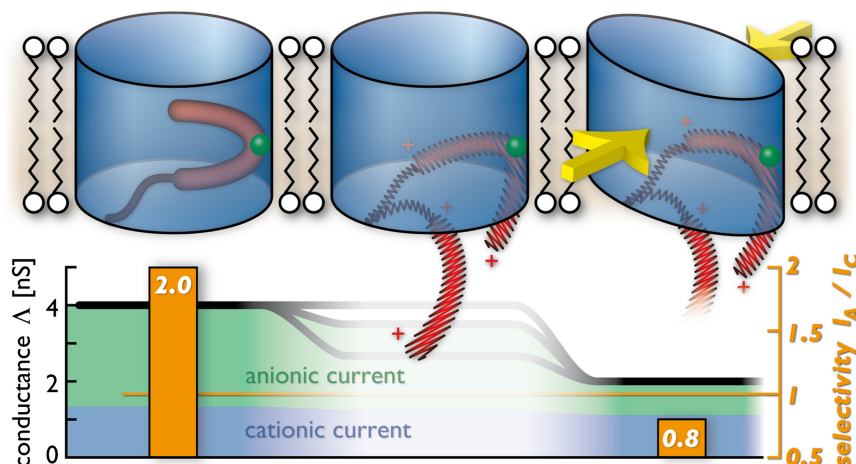
Figure 6. Suggested Model of VDAC Voltage-Induced Gating

At zero transmembrane potential, the VDAC pore (blue) most likely remains in the open state (upper, left). Increasing the membrane voltage beyond ± 30 mV (center) exerts a force on the N-terminal helix (red), which is attached to the barrel wall by the contact residue L10 (green). Detachment or removal of the N-terminal helix from the barrel wall at the L10-V143 contact leaves behind a labile, hull-like pore structure (right) which is more susceptible to undergo (semi)collapse under membrane stress. At an ellipticity of 0.47, the semicollapsed barrel geometry displays the conductance and ion selectivity found experimentally for the wild-type closed state (lower, right), whereas our calculations reproduce the wild-type open state values for noncollapsed structures containing the N-terminal helix (lower, left). Note that semicollapse can also occur under membrane stress when the helix is not removed yet with a smaller probability. Hatching of the N-terminal region in the upper central and right panels indicates that the conformation of a possibly detached N terminus is not known.

patch formed by residues in β strands 9 and 10, was mutated to cysteine and covalently linked to Cys170 (mutated from alanine) in β strand 11. Thus, although covalently linking barrel and N terminus on the one hand, these mutations, on the other hand, disrupted the hydrophobic contact between residues Leu10, Val143, and Leu150 in a similar manner as our L10N mutation. This may offer an explanation for the facilitation of gating which was observed in the L10C-A170C mutant at positive voltages even if no explicit crosslinking was employed. Importantly, the ion selectivity of the crosslinked mVDAC1 mutant was not reported. Our data strongly suggest that the switch to cation selectivity observed in the closed state of VDAC1 does not occur if the N terminus remains within a semicollapsed β-barrel, as also the charge distribution within the N terminus indicates. Thus, a movement of the N-terminal helix out of the β-barrel, possibly in conjunction with segments of the barrel (Peng et al., 1992; Song et al., 1998; Teijido et al., 2012), may be necessary to explain all aspects of VDAC1 gating observed experimentally.

In summary, our data show that destabilization of the link between N terminus and β-barrel facilitates entry of VDAC1 into partially collapsed states which can explain the conductance and selectivity of the closed state. The exposed and charged nature of the N terminus, its stabilizing role for the β-barrel, and the loss of voltage gating in its absence thus suggest that it functions as a switch in the gating process. The model we propose relies on observations made in a large number of experimental and computational studies. These—present and previous—data indicate that the N-terminal helix of VDAC serves as a voltage-dependent sensor and that the cylindrical β-barrel can undergo drastic conformational changes coupled to its membrane environment, in particular when the helix loses its rigid resting conformation (Mannella, 1997; Song et al., 1998; Thomas et al., 1993). The resulting elliptic pores show a wide range of subconductance states with varying selectivity, including cation-selective conformations, in agreement with previous experimental data (Benz, 1994; Colombini, 1989, 2004). Our model extends an earlier suggestion on the gating mechanism of VDAC, made before its atomic structure was

available on the basis of electron microscopic images (Mannella, 1997, 1998), and explains the long-standing observation that gating is pressure-dependent and involves a large volume change of the channel (Zimmerberg and Parsegian, 1986). The scenario we propose implies that the conductance state of VDAC is mechanosensitive, that is, responds to changes in membrane osmotic pressure, as has indeed been observed (Zimmerberg and Parsegian, 1986).

Our results also shed light on the structure and dynamics of β-barrel membrane proteins in general. We show that the geometry of a β-barrel can in fact be very labile, and, as noted before, its dynamics can be sensitive to changes in the lipid environment (Villinger et al., 2010). This agrees well with the observation that VDAC gating can be influenced by osmotic pressure (Zimmerberg and Parsegian, 1986) as well as by lipids that modify membrane lateral pressure (Rostovtseva et al., 2006). Importantly, in many cases, the gating process in bacterial porins has also been reported to be sensitive to membrane pressure in addition to voltage (Lakey and Pattus, 1989; Le Dain et al., 1996). On a wider perspective, our results thus suggest that a closing mechanism by semicollapse may be a general feature of β-barrel proteins.

EXPERIMENTAL PROCEDURES

hVDAC1 was expressed, refolded, and purified in accordance with the protocol described in Engelhardt et al., 2007. For solid-state NMR measurements, the protein was reconstituted into DMPC liposomes at a protein/lipid ratio of 1/50 (mol/mol). Solid-state NMR experiments were conducted using 3.2 or 4 mm triple-resonance (^{1}H,^{13}C,^{15}N) magic-angle spinning (MAS) probeheads at static magnetic fields of 18.8 and 20.0 T (Bruker Biospin, Karlsruhe, Germany). Sample temperature was +5°C. For measurement of dynamics, double quantum – single quantum (2Q,1Q) correlation spectra were recorded employing the SPC5 pulse sequence (Hohwy et al., 1999) as described previously (Schneider et al., 2010b). Spectra were processed in Topspin (Bruker Biospin, Karlsruhe, Germany) and analyzed using Sparky (T.D. Goddard and D.G. Kneller, SPARKY 3, University of California, San Francisco, USA) and MATLAB (The MathWorks, Natick, MA, USA).

The method used for the black lipid bilayer experiments has been described previously (Benz et al., 1978; Roos et al., 1982). Membranes were formed from

a 1% (w/v) solution of diphytanoyl phosphatidylcholine (Avanti, Polar Lipids, Alabaster, AL, USA) in n-decane by painting onto a circular hole (surface area about 0.4 mm^2) separating the two compartments of a Teflon cell. For standard single channel measurements, the Teflon chamber was filled with an unbuffered 1 M KCl solution. The temperature used was 20°C. The voltage across the membrane was applied through silver/silver chloride electrodes (with salt bridges). hVDAC1 and its mutants were added in concentrations of 10 or 100 ng/ml.

All MD simulations were based on the crystal structure of murine VDAC1 (mVDAC1, pdb code 3EMN; Ujwal et al., 2008), whose sequence is 99% identical with that of human VDAC1 (hVDAC1), differing in only four sequence positions (Thr55Asn, Met129Val, Ala160Ser, and Ile227Val). For equilibrium simulations, WT-mVDAC1, Δ(1–20)-mVDAC1, and L10N-mVDAC1 were each inserted in simulation boxes with a fully hydrated and equilibrated membrane consisting of 176 dimyristoylphosphatidylcholine (DMPC) molecules and about 13,000 water molecules using the tool g_membed (Wolf et al., 2010). The amber99sb force field was used for the protein and ions (Hornak et al., 2006), and parameters for DMPC were derived from Berger et al., 1997. The solvent was modeled using the SPC/E water model (Berendsen et al., 1987). All simulations were carried out with the Gromacs simulation software, version 4 (Hess et al., 2008). Simulation of ion flux through WT-mVDAC1 and Δ(1–20)-mVDAC1 and calculation of conductance and ion selectivity values were based on the computational electrophysiology method implemented in Gromacs 4.5 (Kutzner et al., 2011).

More detailed experimental procedures are available in the Supplemental Experimental Procedures.

SUPPLEMENTAL INFORMATION

Supplemental Information includes four figures, one table, and Supplemental Experimental Procedures and can be found with this article online at http://dx.doi.org/10.1016/j.str.2012.06.015.

ACKNOWLEDGMENTS

REFERENCES

Abu-Hamad, S., Arbel, N., Calo, D., Arzoine, L., Israelson, A., Keinan, N., Ben-Romano, R., Friedman, O., and Shoshan-Barmatz, V. (2009). The VDAC1 N-terminus is essential both for apoptosis and the protective effect of anti-apoptotic proteins. J. Cell Sci. 122, 1906–1916.

Ader, C., Schneider, R., Hornig, S., Velisetty, P., Wilson, E.M., Lange, A., Giller, K., Ohmert, I., Martin-Eauclaire, M.F., Trauner, D., et al. (2008). A structural link between inactivation and block of a K$^+$ channel. Nat. Struct. Mol. Biol. 15, 605–612.

Bayrhuber, M., Meins, T., Habeck, M., Becker, S., Giller, K., Villinger, S., Vonrhein, C., Griesinger, C., Zweckstetter, M., and Zeth, K. (2008). Structure of the human voltage-dependent anion channel. Proc. Natl. Acad. Sci. USA 105, 15370–15375.

Benz, R. (1994). Permeation of hydrophilic solutes through mitochondrial outer membranes: review on mitochondrial porins. Biochim. Biophys. Acta 1197, 167–196.

Benz, R., Janko, K., Boos, W., and Läuger, P. (1978). Formation of large, ion-permeable membrane channels by the matrix protein (porin) of Escherichia coli. Biochim. Biophys. Acta 511, 305–319.

Benz, R., Maier, E., Thinnes, F.P., Götz, H., and Hilschmann, N. (1992). Studies on human porin. VII. The channel properties of the human B-lymphocyte membrane-derived "Porin 31HL" are similar to those of mitochondrial porins. Biol. Chem. Hoppe Seyler 373, 295–303.

Berendsen, H.J.C., Grigera, J.R., and Straatsma, T.P. (1987). The missing term in effective pair potentials. J. Phys. Chem. 91, 6269–6271.

Berger, O., Edholm, O., and Jähnig, F. (1997). Molecular dynamics simulations of a fluid bilayer of dipalmitoylphosphatidylcholine at full hydration, constant pressure, and constant temperature. Biophys. J. 72, 2002–2013.

Choudhary, O.P., Ujwal, R., Kowallis, W., Coalson, R., Abramson, J., and Grabe, M. (2010). The electrostatics of VDAC: implications for selectivity and gating. J. Mol. Biol. 396, 580–592.

Colombini, M. (1989). Voltage gating in the mitochondrial channel, VDAC. J. Membr. Biol. 111, 103–111.

Colombini, M. (2004). VDAC: the channel at the interface between mitochondria and the cytosol. Mol. Cell. Biochem. 256-257, 107–115.

Cowan, S.W., Schirmer, T., Rummel, G., Steiert, M., Ghosh, R., Pauptit, R.A., Jansonius, J.N., and Rosenbusch, J.P. (1992). Crystal structures explain functional properties of two E. coli porins. Nature 358, 727–733.

Dargent, B., Hofmann, W., Pattus, F., and Rosenbusch, J.P. (1986). The selectivity filter of voltage-dependent channels formed by phosphoporin (PhoE protein) from E. coli. EMBO J. 5, 773–778.

De Pinto, V., Prezioso, G., Thinnes, F., Link, T.A., and Palmieri, F. (1991). Peptide-specific antibodies and proteases as probes of the transmembrane topology of the bovine heart mitochondrial porin. Biochemistry 30, 10191–10200.

De Pinto, V., Tomasello, F., Messina, A., Guarino, F., Benz, R., La Mendola, D., Magrì, A., Milardi, D., and Pappalardo, G. (2007). Determination of the conformation of the human VDAC1 N-terminal peptide, a protein moiety essential for the functional properties of the pore. ChemBioChem 8, 744–756.

De Pinto, V., Reina, S., Guarino, F., and Messina, A. (2008). Structure of the voltage dependent anion channel: state of the art. J. Bioenerg. Biomembr. 40, 139–147.

Engelhardt, H., Meins, T., Poynor, M., Adams, V., Nussberger, S., Welte, W., and Zeth, K. (2007). High-level expression, refolding and probing the natural fold of the human voltage-dependent anion channel isoforms I and II. J. Membr. Biol. 216, 93–105.

Guo, X.W., Smith, P.R., Cognon, B., D'Arcangelis, D., Dolginova, E., and Mannella, C.A. (1995). Molecular design of the voltage-dependent, anion-selective channel in the mitochondrial outer membrane. J. Struct. Biol. 114, 41–59.

Haltia, T., and Freire, E. (1995). Forces and factors that contribute to the structural stability of membrane proteins. Biochim. Biophys. Acta 1241, 295–322.

Hess, B., Kutzner, C., van der Spoel, D., and Lindahl, E. (2008). GROMACS 4: algorithms for highly efficient, load-balanced, and scalable molecular simulation. J. Chem. Theory Comput. 4, 435–447.

Hiller, S., Garces, R.G., Malia, T.J., Orekhov, V.Y., Colombini, M., and Wagner, G. (2008). Solution structure of the integral human membrane protein VDAC-1 in detergent micelles. Science 321, 1206–1210.

Hiller, S., Abramson, J., Mannella, C., Wagner, G., and Zeth, K. (2010). The 3D structures of VDAC represent a native conformation. Trends Biochem. Sci. 35, 514–521.

Hirn, R., Benz, R., and Bayerl, T.M. (1999). Collective membrane motions in the mesoscopic range and their modulation by the binding of a monomolecular protein layer of streptavidin studied by dynamic light scattering. Phys. Rev. E 59 (5 Pt B), 5987–5994.

Hohwy, M., Rienstra, C.M., Jaroniec, C.P., and Griffin, R.G. (1999). Fivefold symmetric homonuclear dipolar recoupling in rotating solids: application to double quantum spectroscopy. J. Chem. Phys. 110, 7983–7992.

Hornak, V., Abel, R., Okur, A., Strockbine, B., Roitberg, A., and Simmerling, C. (2006). Comparison of multiple Amber force fields and development of improved protein backbone parameters. Proteins *65*, 712–725.

Hunte, C., and Richers, S. (2008). Lipids and membrane protein structures. Curr. Opin. Struct. Biol. *18*, 406–411.

Kutzner, C., Grubmüller, H., de Groot, B.L., and Zachariae, U. (2011). Computational electrophysiology: the molecular dynamics of ion channel permeation and selectivity in atomistic detail. Biophys. J. *101*, 809–817.

Lakey, J.H., and Pattus, F. (1989). The voltage-dependent activity of Escherichia coli porins in different planar bilayer reconstitutions. Eur. J. Biochem. *186*, 303–308.

Le Dain, A.C., Häse, C.C., Tommassen, J., and Martinac, B. (1996). Porins of Escherichia coli: unidirectional gating by pressure. EMBO J. *15*, 3524–3528.

Lee, K.I., Rui, H., Pastor, R.W., and Im, W. (2011). Brownian dynamics simulations of ion transport through the VDAC. Biophys. J. *100*, 611–619.

Mannella, C.A. (1997). Minireview: on the structure and gating mechanism of the mitochondrial channel, VDAC. J. Bioenerg. Biomembr. *29*, 525–531.

Mannella, C.A. (1998). Conformational changes in the mitochondrial channel protein, VDAC, and their functional implications. J. Struct. Biol. *121*, 207–218.

Martinac, B., Buechner, M., Delcour, A.H., Adler, J., and Kung, C. (1987). Pressure-sensitive ion channel in Escherichia coli. Proc. Natl. Acad. Sci. USA *84*, 2297–2301.

Nietlispach, D., and Gautier, A. (2011). Solution NMR studies of polytopic α-helical membrane proteins. Curr. Opin. Struct. Biol. *21*, 497–508.

Peng, S., Blachly-Dyson, E., Forte, M., and Colombini, M. (1992). Large scale rearrangement of protein domains is associated with voltage gating of the VDAC channel. Biophys. J. *62*, 123–131, discussion 131–135.

Perozo, E., Cortes, D.M., Sompornpisut, P., Kloda, A., and Martinac, B. (2002). Open channel structure of MscL and the gating mechanism of mechanosensitive channels. Nature *418*, 942–948.

Phillips, R., Ursell, T., Wiggins, P., and Sens, P. (2009). Emerging roles for lipids in shaping membrane-protein function. Nature *459*, 379–385.

Pongprayoon, P., Beckstein, O., Wee, C.L., and Sansom, M.S. (2009). Simulations of anion transport through OprP reveal the molecular basis for high affinity and selectivity for phosphate. Proc. Natl. Acad. Sci. USA *106*, 21614–21618.

Popp, B., Court, D.A., Benz, R., Neupert, W., and Lill, R. (1996). The role of the N and C termini of recombinant Neurospora mitochondrial porin in channel formation and voltage-dependent gating. J. Biol. Chem. *271*, 13593–13599.

Roos, N., Benz, R., and Brdiczka, D. (1982). Identification and characterization of the pore-forming protein in the outer membrane of rat liver mitochondria. Biochim. Biophys. Acta *686*, 204–214.

Rostovtseva, T.K., Kazemi, N., Weinrich, M., and Bezrukov, S.M. (2006). Voltage gating of VDAC is regulated by nonlamellar lipids of mitochondrial membranes. J. Biol. Chem. *281*, 37496–37506.

Rui, H., Lee, K.I., Pastor, R.W., and Im, W. (2011). Molecular dynamics studies of ion permeation in VDAC. Biophys. J. *100*, 602–610.

Runke, G., Maier, E., Summers, W.A.T., Bay, D.C., Benz, R., and Court, D.A. (2006). Deletion variants of Neurospora mitochondrial porin: electrophysiological and spectroscopic analysis. Biophys. J. *90*, 3155–3164.

Schindler, H., and Rosenbusch, J.P. (1981). Matrix protein in planar membranes: clusters of channels in a native environment and their functional reassembly. Proc. Natl. Acad. Sci. USA *78*, 2302–2306.

Schmidt, D., and MacKinnon, R. (2008). Voltage-dependent K+ channel gating and voltage sensor toxin sensitivity depend on the mechanical state of the lipid membrane. Proc. Natl. Acad. Sci. USA *105*, 19276–19281.

Schneider, R., Etzkorn, M., Giller, K., Daebel, V., Eisfeld, J., Zweckstetter, M., Griesinger, C., Becker, S., and Lange, A. (2010a). The native conformation of the human VDAC1 N terminus. Angew. Chem. Int. Ed. Engl. *49*, 1882–1885.

Schneider, R., Seidel, K., Etzkorn, M., Lange, A., Becker, S., and Baldus, M. (2010b). Probing molecular motion by double-quantum (13C,13C) solid-state NMR spectroscopy: application to ubiquitin. J. Am. Chem. Soc. *132*, 223–233.

Shoshan-Barmatz, V., Keinan, N., and Zaid, H. (2008). Uncovering the role of VDAC in the regulation of cell life and death. J. Bioenerg. Biomembr. *40*, 183–191.

Shoshan-Barmatz, V., De Pinto, V., Zweckstetter, M., Raviv, Z., Keinan, N., and Arbel, N. (2010). VDAC, a multi-functional mitochondrial protein regulating cell life and death. Mol. Aspects Med. *31*, 227–285.

Song, J., Midson, C., Blachly-Dyson, E., Forte, M., and Colombini, M. (1998). The sensor regions of VDAC are translocated from within the membrane to the surface during the gating processes. Biophys. J. *74*, 2926–2944.

Sukharev, S. (2002). Purification of the small mechanosensitive channel of Escherichia coli (MscS): the subunit structure, conduction, and gating characteristics in liposomes. Biophys. J. *83*, 290–298.

Teijido, O., Ujwal, R., Hillerdal, C.O., Kullman, L., Rostovtseva, T.K., and Abramson, J. (2012). Affixing the N-terminal alpha helix of the voltage dependent anion channel to the channel's wall does not prevent its voltage gating. J. Biol. Chem. *287*, 11437–11445.

Thomas, L., Blachly-Dyson, E., Colombini, M., and Forte, M. (1993). Mapping of residues forming the voltage sensor of the voltage-dependent anion-selective channel. Proc. Natl. Acad. Sci. USA *90*, 5446–5449.

Tieleman, D.P., and Berendsen, H.J. (1998). A molecular dynamics study of the pores formed by Escherichia coli OmpF porin in a fully hydrated palmitoyloleoylphosphatidylcholine bilayer. Biophys. J. *74*, 2786–2801.

Ujwal, R., Cascio, D., Colletier, J.P., Faham, S., Zhang, J., Toro, L., Ping, P.P., and Abramson, J. (2008). The crystal structure of mouse VDAC1 at 2.3 A resolution reveals mechanistic insights into metabolite gating. Proc. Natl. Acad. Sci. USA *105*, 17742–17747.

Villinger, S., Briones, R., Giller, K., Zachariae, U., Lange, A., de Groot, B.L., Griesinger, C., Becker, S., and Zweckstetter, M. (2010). Functional dynamics in the voltage-dependent anion channel. Proc. Natl. Acad. Sci. USA *107*, 22546–22551.

Wimley, W.C. (2003). The versatile beta-barrel membrane protein. Curr. Opin. Struct. Biol. *13*, 404–411.

Wolf, M.G., Hoefling, M., Aponte-Santamaría, C., Grubmüller, H., and Groenhof, G. (2010). g_membed: Efficient insertion of a membrane protein into an equilibrated lipid bilayer with minimal perturbation. J. Comput. Chem. *31*, 2169–2174.

Young, M.J., Bay, D.C., Hausner, G., and Court, D.A. (2007). The evolutionary history of mitochondrial porins. BMC Evol. Biol. *7*, 31.

Zachariae, U., Klühspies, T., De, S., Engelhardt, H., and Zeth, K. (2006). High resolution crystal structures and molecular dynamics studies reveal substrate binding in the porin Omp32. J. Biol. Chem. *281*, 7413–7420.

Zaid, H., Abu-Hamad, S., Israelson, A., Nathan, I., and Shoshan-Barmatz, V. (2005). The voltage-dependent anion channel-1 modulates apoptotic cell death. Cell Death Differ. *12*, 751–760.

Zimmerberg, J., and Parsegian, V.A. (1986). Polymer inaccessible volume changes during opening and closing of a voltage-dependent ionic channel. Nature *323*, 36–39.

Note Added in Proof

Very recently, Griffin and coworkers have published a solid-state NMR study on 2D crystals of hVDAC1 (Eddy et al., 2012). Interestingly, the spectra of hVDAC1 in the 2D crystals and in liposomes as studied by us are quite similar, which indicates that the structure of hVDAC1 is conserved in the different environments. Importantly, the study on 2D crystals fully confirmed our obtained resonance assignments for the N-terminal residues of hVDAC1 in lipid bilayers and also corroborates the rigid nature of the N terminus under various experimental conditions (lipid composition and temperature).

Eddy, M.T., Ong, T.-C., Clark, L., Teijido, O., van der Wel, P.C.A., Garces, R., Wagner, G., Rostovtseva, T.K., Griffin, R.G. (2012). Lipid dynamics and protein-lipid interactions in 2D crystals formed with the beta-barrel integral membrane protein VDAC1. J. Am. Chem. Soc. *134*, 6375–6387.